Chemistry Africa
https://doi.org/10.1007/s42250-023-00769-2

ORIGINAL ARTICLE

Ruthenium Polypyridyl Complexes with Hydroxypyridine: Experimental, DFT Studies, and In Silico Antitubercular Activity Investigation

Abdullahi O. Rajee[1] · Joshua A. Obaleye[1] · Hitler Louis[2,7] · Sheriff O. Ayinla[3] · Abdulbasit A. Aliyu[4] · Wahab A. Osunniran[5] · Amudat Lawal[1] · Gideon E. Mathias[2] · Michael E. Rasaki[2] · Amanda-Lee E. Manicum[6]

Received: 15 March 2023 / Accepted: 16 August 2023
© The Tunisian Chemical Society and Springer Nature Switzerland AG 2023

Abstract

This study reports the synthesis, spectroscopic, molecular properties, and in silico biological assessment of ruthenium polypyridyl complexes with a hydroxypyridine ligand, $[Ru(bpy)_2(N\text{^}O)](PF_6)$ (**Ru-1**) and $[Ru(phen)_2(N\text{^}O)](PF_6)$ (**Ru-2**). The compounds have been characterized by FT-IR, UV, single crystal X-ray crystallography while molecular electronic properties have been considered within the framework of density functional theory (DFT) computation. The explicit interpretation of the vibrational spectra was assigned by the VEDA4e program. The results obtained from the natural bond analysis explicated that the highest stabilization energy $E^{(2)}$ for the Ru-2 molecule is 343.53 kcal/mol while the Ru-1 compound was observed to possess $E^{(2)}$ energy of 302.42 kcal/mol. The studied Ru-2 compound has been observed to exhibit high gastrointestinal absorption which might restrict the brain-blood barrier or any cytochrome p450 inhibition (1A2, 2C19, 3A4, and 3A4) without infringing any of the Lipniski rules. The molecular docking experiment reveal that the Ru-2 compound binds effectively with 2nv6 tuberculosis receptor with a corresponding binding affinity of − 8.6 kcal/mol obtained for Ru-1 molecule. However, when both compounds were docked with the 5syj receptor, the binding affinity was observed to be − 7.5 and − 6.7 kcal/mol for Ru-2 and Ru-1 respectively, which is comparably higher than the binding score observed for isoniazid standard drug. Ru-2 complex was observed to possess a high energy gap of 2.948 eV with a chemical softness of 0.678 eV, thus suggesting the studied molecule is highly stable and suitable and can be used as a potential anti-tubercular agent. The Uv–vis spectroscopy study divulged that all absorption spectra occurred at the visible region for both molecules respectively, which is in tandem with the obtained experimental λ_{max}.

Keywords Ruthenium · Single crystal X-ray crystallography · DFT · Molecular-docking · Antituberculosis

✉ Abdullahi O. Rajee
olarajee@unilorin.edu.ng

[1] Department of Chemistry, Faculty of Physical Sciences, University of Ilorin, Ilorin, Nigeria

[2] Computational and Bio-Simulation Research Group, University of Calabar, Calabar, Nigeria

[3] Department of Chemical and Geological Sciences, Al-Hikmah University, Ilorin, Nigeria

[4] Department of Pure and Industrial Chemistry, Kogi State University, Anyigba, Kogi, Nigeria

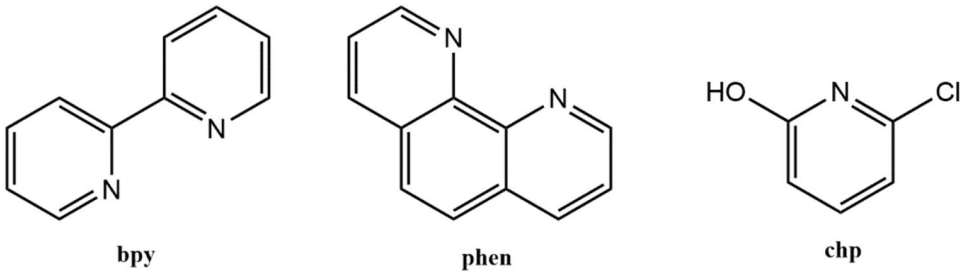
[5] Department of Chemical, Geological and Physical Sciences, Kwara State University, P. M. B. 1530, Malete, Ilorin, Nigeria

[6] Department of Chemistry, Tshwane University of Technology, Pretoria, South Africa

[7] Centre for Herbal Pharmacology and Environmental Sustainability, Chettinad Hospital and Research Institute, Chettinad Academy of Research and Education, Kelambakkam, Tamil Nadu 603103, India

Published online: 31 August 2023

Scheme 1 The chemical structures of bpy, phen and chp ligand



1 Introduction

Mycobacterium tuberculosis is known to be the most common strain causing tuberculosis, a potentially dangerous infectious bacterial illness that mostly affect the lungs of infected host. However, it has been observed to also have adverse effect on other regions of the human body [1, 2]. Analysis have shown that about one third of the world's population is afflicted with TB, which accounts for over 4000 fatalities per day and thus ranks second only to the human immunodeficiency virus (HIV) as a cause of mortality that may be transmitted [3]. Due to the difficulty of treatment, many antibiotics must be administered over an extended period of time. As such, with the emergence of mycobacterium tuberculosis, bacteria strains that are multi-drug resistant have intrigued researchers to sort developing new TB drugs with a more effective performance. Interestingly, a plethora of possibilities for creating molecules with higher bioactivity profile are provided using metal complexes. This is made feasible by the accessibility of various metal ions as well as with the capacity to modify structures through ligand exchange. The interaction between the metal's activity and that of its organic ligand may disclose novel mechanism of action, which is mainly due to their photophysical, stability and electrochemical characteristics of ruthenium complexes as they seem to have captivated interest and are constantly being studied for application in dye-sensitized solar cells, photocatalysis, organic light-emitting diodes, as well as biological applications [4, 5]. These inbuilt properties of ruthenium complexes make it fit for pharmacological uses. Ru-drug is observed to possess a decreased systemic toxicity which accounts more for its experimental advantage. It is observed that the ruthenium complexes tuneable oxidation states, DNA-binding capacity, hydrophobicity and lipophilicity can be regulated through the use of various organic compounds (Ligands). The cytotoxicity of Ru(II) polypyridyl complexes is significantly influenced by lipophilicity as well as cellular absorption. This development may lead to alteration in the biological pharmaceutical application [6, 7] of the compound. The ligand frame work, metal ions selection, as well as metal ions oxidation state all play a role in the design of metal-based medicines. In attempt to curb the aforementioned challenge, researchers have focused on the synthesis and assessment of the biologically interesting ligands, with the sine qua non of broadening the spectrum of complex activity. The biological activity of a complex is thus strongly dependent on the coordination behaviour of the metal.

Due to the high cytotoxicity, selectivity and moderate toxicity, ruthenium complexes have recently received a whole lot of attention as potential anti-bacterial and anti-cancer therapy [6–8]. Pyridine derivative are frequently utilized as ligands in the synthesis of coordination compounds that are often used as pharmaceuticals. The biological effects of pyridine derivative basically involve the well-known anti-tubercular, anthelmintic, fungicidal, anti-cancer and anti-bacterial action. Thus, pyridine-based ruthenium complexes hold a promising potency for optical cell imaging [8]. Furthermore, ruthenium compounds together with pyridine have been observed to effectively inhibit the growth of bacterial biofilm as well as induce apoptosis in cancerous cells [9–11]. In other to understand in detail about the capabilities of Ru polypyridyl complexes, the synthesis of Ru(II) monocationic compounds with N–O donor ligands with pi extended system was investigated. To consider the direct link between hydrophobicity, cellular absorption and cytotoxic action, $[Ru^{II} N_5O]^+$ pseudo-octahedral coordination environment was utilized for these purposes. A distinct class of anti-tubercular Ru complexes was suggested to be produced via the addition of a lipophilic N–O bidentate ligand. $[Ru(bpy)_2(chp)][PF_6]$ (Ru-1) and $[Ru(phen)_2(chp)][PF_6]$ (Ru-2) Ru complexes were synthesized for this series (bpy = 2, 2-bipyridine, phen = 1, 10- phenanthroline, and chp = 2-chloro-6-hydroxy pyridine) (Scheme 1). To enhance our studies on the Ru-complexes, density functional theoretical method was employed to empirically and theoretically account for the anti-tubercular activity of the investigated ruthenium polypyridyl complexes. Nevertheless, to lucidly provide additional detailed structural information on the potency of the studied organic molecules to exhibit anti-tubercular activity, the investigated complexes were experimentally produced and characterized using single crystal X-ray crystallography, NMR, UV–Vis and FT-IR, and thus our intriguing findings are disclosed herein.

2 Experimental

2.1 Materials and Methods

The compounds were created using the normal Schlenk-line technique under anaerobic conditions (N_2 atmosphere). The solvent used was basically of the reagent grade kind. The following organic molecules were bought and equally utilized exactly as directed; $RuCl_3.XH_2O$ (pressure chemicals), 2,2-bipyridine (bpy, Afa Aesar), 1, 10-phenanthroline (phen, Alfa Aesar), NH_4PF_6 (Sigma Aldrich), and K_2CO_3 (spectrum). The chemicals employed for the synthesis were of analytical quality and hence conventionally utilized exactly as received. At Atlantic Microlab, Inc., elemental analyses were performed. (N or cross, GA). A Shimadzu UVPC-3001 spectrophotometer was adopted to collect the absorption spectra of the investigated compounds [12]. Having the given sample primarily composed of KBr pellet, infrared spectra were performed through a Perkin-Elmer FT-IR spectrophotometer spectrum 2000.

2.2 Synthesis of Chp Complexes

$[Ru(bpy)_2Cl_2].2H_2O$ or **Ru-1** was prepared by a reported literature method [13]. $[Ru(bpy)_2Cl_2].2H_2O$ (100 mg, 0.192 mmol) was dissolved in EtOH/H_2O (10 mL) (50:50) to give a purple solution. 2-chloro-6-hydroxypyridine, chp (0.030 g, 0.231 mmol) was added to the stirring solution followed by the addition of aqueous solution of K_2CO_3 (0.032 g, 0.163 mmol) dropwise to give a dark red solution. The reaction was setup for reflux at 90 °C for 8 h. The solution was then reduced to ~ 2 mL by rotary evaporation after which the product was precipitated with excess aqueous NH_4PF_6 (0.157 g, 0.960 mmol). It was filtered and washed with Et_2O to afford a dark red powder which was dried overnight and then isolated. **Yield** = 86% (0.120 g) **^{1}H NMR** (300 MHz, CD_3COCD_3) δ 9.10 (ddd, J = 5.6, 1.5, 0.8 Hz, 1H), 8.65 (ddd, J = 5.6, 1.5, 0.8 Hz, 1H), 8.56 (m, 3H), 7.74 (dt, J = 4.6, 1.4 Hz, 2H), 7.72 (m, 1H), 7.68 (dd, J = 2.0, 1.4 Hz, 1H), 7.66 (d, J = 1.3 Hz, 1H), 7.63 (ddd, J = 5.7, 1.5, 0.8 Hz, 1H), 7.41 (m, 1H), 7.20 (m, 1H), 7.12 (m, 2H), 6.38 (dd, J = 7.7, 0.7 Hz, 1H), 6.04 (dd, J = 8.5, 0.7 Hz, 1H). **ESI–MS** (m/z) = 542.030 $[M\text{-}PF_6]^+$.

Also 100 mg, 0.136 mmol of $[Ru(phen)_2Cl_2]0.2H_2O$ or **Ru-2** molecule was dissolved in EtOH/H_2O (10 mL) (50:50) to give a purple solution. The White powder of 2-chloro-6-hydroxypyridine (0.021 g, 0.163 mmol) was added to the stirring solution followed by the addition of aq. solution of K_2CO_3 (0.023 g, 0.163 mmol) dropwise to give a dark red solution. The reaction was set up for reflux at 90 °C for 8 h. The solution was then reduced to 2 mL by rotary evaporation after which the product was precipitated with excess aq. NH_4PF_6 (0.111 g, 0.680 mmol). It was filtered and washed with Et_2O to afford a dark red powder which was dried overnight and then isolated. **Yield** = 87% (0.092 g) **^{1}H NMR** (300 MHz, CD_3COCD_3) δ 10.04 (dd, J = 5.3, 1.2 Hz, 1H), 9.96 (dd, J = 5.2, 1.3 Hz, 1H), 9.50 (dd, J = 5.2, 1.3 Hz, 4H), 9.09 (dd, J = 5.2, 1.1 Hz, 4H), 8.72 (dd, J = 7.9, 6.2 Hz, 9H), 8.32 (m, 12H), 8.24 (s, 8H), 8.13 (s, 5H), 8.12 (m, 13H), 7.88 (dd, J = 17.7, 4.9 Hz, 9H), 7.75 (dd, J = 5.3, 1.2 Hz, 1H), 7.70 (dd, J = 5.3, 1.2 Hz, 1H), 7.42 (m, 16H), 6.88 (dd, J = 8.2, 7.3 Hz, 1H), 6.35 (dd, J = 7.7, 0.6 Hz, 4H), 6.10 (ddd, J = 17.8, 8.4, 0.6 Hz, 5H), 5.88 (s, 1H). **ESI–MS** (m/z) = 590.032 $[M\text{-}PF_6]^+$

2.3 Single Crystal X-ray Crystallographic Procedure

A single crystal X-ray diffraction method was employed to effectively ascertain the crystal structure of Ru-2. To obtain the desired single crystal of the complex, slow diffusion of diethyl ether into an acetonitrile solution of the compound at room temperature was carried out. Using a Burker APEX II CCD diffractometer, data for the studied complexes were obtained, and this was achieved by utilizing a graphite monochromated Mo–Ka radiation, with λ= 0.71073 Å at 90 K. A minute layer of paratone-N oil was employed to be able to place the crystal on a mylarloop. Then the APEX2 software was used to perform a 60-s scan that was of great use, in that it provides sufficient data on the level of intensity, which would be of importance to analyze using SAINT and corrected for absorption using SADABS [14]. The direct technique was then carried out to carefully dissolve the structure before full-matrix least squares versus F2 and Table 1 were used to improve the compound alongside anisotropic displacement parameters for the non-hydrogen atoms via the SHELXS as well as SHELXL program package correspondingly [15] (Table 1).

2.3.1 Computational Methodology

The synthesized ruthenium polypyridyl complexes (Ru-1 and Ru-2) underwent further computational analysis using Gaussian 16 software and GaussView 6.0.16 interface to affirm the stability as well as to comprehend the molecular geometry of the studied organic molecule [16, 17]. The investigated structures were optimized at a at DFT level, coupling B3LYP [x] functional with a combination of Def2-TZVP [x] triple-ζ basis set and LANL2DZ double-ζ basis set + ECP. More so, D3 version of Grimme's dispersion with Becke-Johnson damping [x] was also included. The predicted molecular geometries were compared with the experimental XRD structures. The stationary points achieved upon geometry optimisation were submitted to the

Table 1 Crystal structural data and refinement parameters for $[Ru(phen)_2(chp)][PF_6]$ ***(2)***

Compound	$[Ru(phen)_2(chp)][PF_6]$ (2)	
Empirical Formula	$C_{31}H_{22}ClF_6N_6OPRu$	
Formula weight	776.03	
Temperature, K	90	
Crystal system	Triclinic	
Space group	P1/c	
Unit cell dimension	a = 8.9343(4) Å	α = 60.9000(10)°
	b = 13.8288(6) Å	β = 86.4190(10)°
	c = 14.1309(6) Å	γ = 77.9730(10)°
Volume, Å^3	1490.47(11)	
Z	2	
Density, g/cm^3	1.729	
Absorption coefficient, mm^{-1}	0.746	
F(000)	776.0	
Crystal colour, morphology	red, block	
Crystal size, mm^3	0.390 × 0.140 × 0.110	
Reflections collected	66,443	
Independent reflections	11,428 [R_{int} = 0.0655, R_{sigma} = 0.0553]	
Data/restraints/parameters	11,428/0/501	
Goodness-of-fit on F^2	1.043	
R indices [I > = 2σ(I)]	R_1 = 0.0410, wR_2 = 0.0766	
R indices (all data)	R_1 = 0.0674, wR_2 = 0.0848	
Largest diff. peak/hole, e/Å^{-3}	0.78/− 0.77	

calculation of vibrational frequencies (in Harmonic approximation) to check whether real minima of the potential energy surface were obtained. The absence of negative frequencies indicates that the optimised structures were genuine minima for the validation of the crystal structure as well as molecular orbitals, Ortep 3 and Avogadro software [18, 19] were employed. Calculations of additional molecular and natural bond orbital (NBO) [x] were carried out at the same level of theory for both studied molecules of interest.

2.3.2 Molecular Docking Procedures

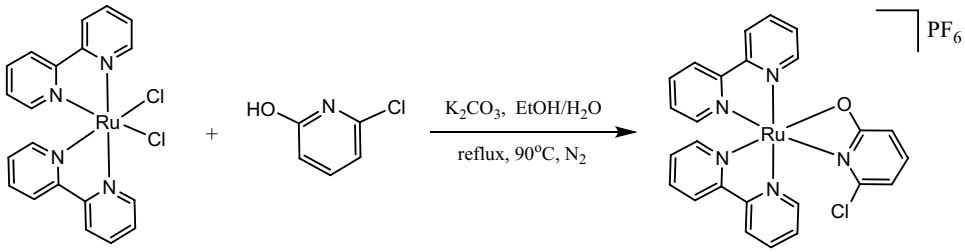
The studied protein was prepared using the Biova Discovery Studio [x], then the selected receptor for molecular docking was imported from online Protein Data Bank [20]. Prior to determining the protein active sites, water molecules were expunged since it has little or no importance, following the addition of explicit hydrogen molecules, which aids in finding the hydrogen bond interactions and more effectual to ascertaining the binding affinity of the investigated ligand against the target protein of interest. In order to specify the protein cavity, its X, Y, Z coordinate were set to − 4.570, 34.7134 and 14.0544 for 2nv6 receptor as well as − 8.8290, − 55.8040, and 35.2730 for 5syj proteins, respectively, with a corresponding size of 20 Å [21]. Autodock 4.0 [x] was employed to convert the initial format of the protein–ligand complex into the required pdbqt file type. Energy minimization at DFT/B3LYP/Gen basis set was used to prepare both the ligands and the standard anti-tuberculosis drug. Thereafter, docking of the proposed ligand with the selected receptor was carried out via Autodock vina and experimental result examined using pymol and Biova Discovery Studio visualizer [22, 23]. Subsequently, the docking exercise were finalized by utilizing the Larmackian Genetic Algorithm with autodock 4.0 and autodock tools (ADT) (LGA). Moreover, it was observed that the autodock grading function is heavily reliant on electrostatic contact, hydrogen binding as well as van der Waals interaction, since these are determining factors that elucidates in details how strong the studied organic compounds bind to the receptor [24]. The docking process's grid parameter file (GPF) was set at 20 × 20 × 20, 20 × 20 × 20 and 20 × 20 × 20 along the systems X, Y, Z coordinate.

3 Results and Discussion

3.1 Synthesis of Complexes

The complexes were synthesized from a reaction of 2-chloro-6-hydroxypyridine, chp with $[Ru(N\hat{}N)_2Cl_2]$ in C_2H_5OH/H_2O in 1:1 molar ratio and were isolated as their PF_6 salts in high yields (Scheme 1 and 2). The ^1H spectra

Scheme 2 Synthesis of $[Ru(bpy)_2Cl_2].2H_2O \cong$ **Ru-1**



of the complexes are given in Figure S (see supplementary material).

3.2 X-ray Structure of Ru-2

Herein, details of the crystallographic data and structure refinement parameters are summarized in Table S1 [25]. The compound crystallizes in the triclinic P1 space group. The complex exhibits an octahedral geometry of the Ru atom. The coordination sphere of the metal center in the structure of Ru-**2** consists of five N atoms and one O atom in a slightly distorted octahedral environment. The Ru– O bond distance is 2.1522(14) Å. Four of the nitrogen atoms from two bipyridyl moiety [26]. The average equatorial Ru–N bond distance for the phenyl is 2.065(15) Å. The hydoxypyridine moiety coordinate the Ru centre via the pyridinic nitrogen and hydroxyl oxygen atom [Ru-N5, 2.0656(16); Ru-O1, 2.1522(14) Å] respectively, forming an octahedral environment round the central Ru atom sphere (Table S2). These distances are comparable and are also in agreement with the respective distances for compounds in a $[RuN_5O]^+$ coordination environment (Fig. 1) (Scheme 3).

3.3 Electronic Properties

Frontier molecular orbital analysis involving the highest occupied and lowest unoccupied molecular orbital (HOMO) and (LUMO) is utilized for the qualitative determination of molecular excitation capacities as well as electron transportation vehicles of the studied molecules [27]. The

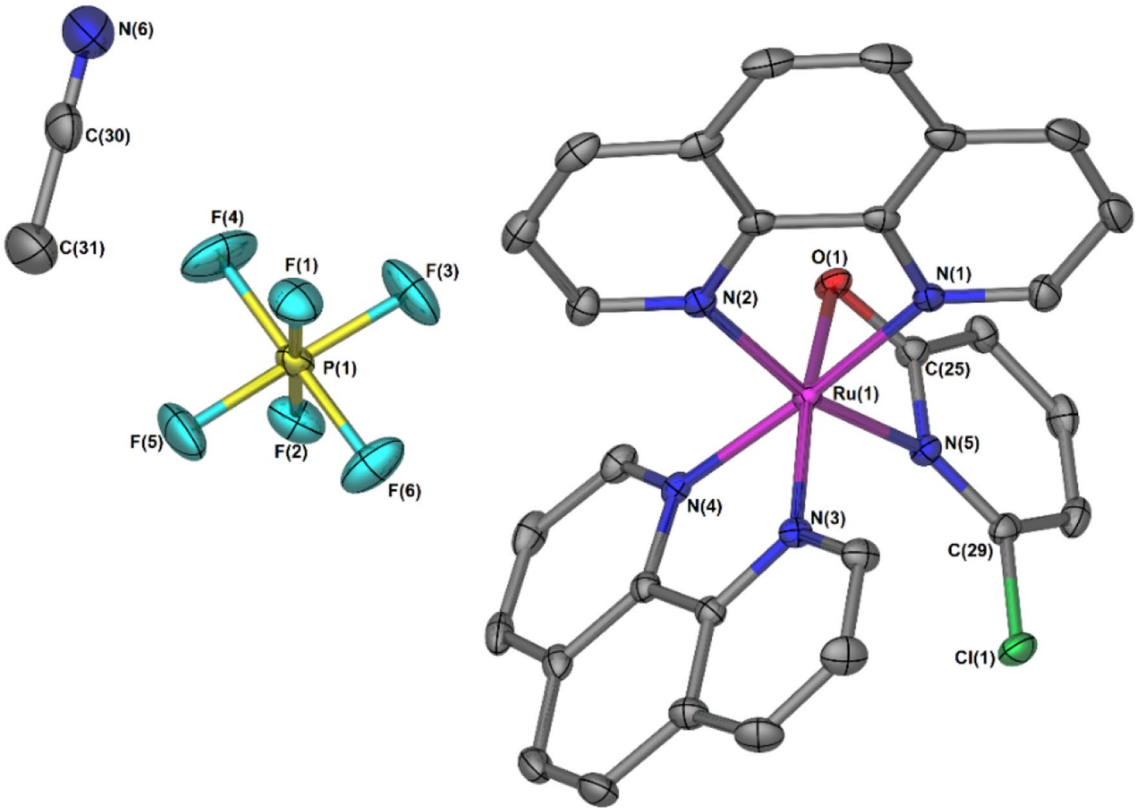
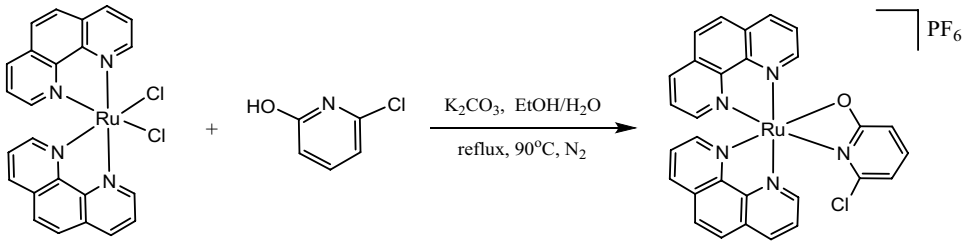


Fig. 1 ORTEP diagram of $[Ru(phen)_2(chp)][PF_6]CH_3CN$, complex 2 showing the atom numbering scheme showing the PF_6 counter ions. Hydrogen atoms are omitted for clarity

Scheme 3 Synthesis of $[Ru(phen)_2Cl_2].2H_2O \cong$ **Ru-2**



discrepancies between the HOMO and LUMO energy levels is substantiated by the presence of energy gap which is the essential parameter that supplies important information in respect to the stability and reactivity of the studied synthesized compounds [28]. The HOMO elucidates the electron donating ability whereas the lowest unoccupied molecular orbital designates the electrophilic capacity of the synthesized compounds [29–31]. So, to say, the molecular chemical reactivity of the complex was blazoned via the HOMO—LUMO energy gap, in affirmation to this justification, it is essential to fathom that high energy gap suggests high kinetic stability as well as low chemical reactivity of the ruthenium polypyridyl complexes (Ru-1 and Ru-2). The electronic properties like HOMO and LUMO energies (E_{HOMO} and E_{LUMO}), energy gap (ΔE), electron affinity (A), global chemical hardness (η), ionization potential energy (IP), global chemical softness (*S*), electronegativity index (**χ**), global chemical electrophilicity index (ω) and chemical potential (μ) were calculated and reported in table? Using equation [1–3, 32]

$$\mathrm{I.P} = -E_{HOMO} \tag{1}$$

$$\mathrm{A} = -E_{LUMO} \tag{2}$$

$$\mu = \frac{IP + EA}{2} \tag{3}$$

$$S = \frac{1}{2\eta} \tag{4}$$

As such, the result divulged that the highest energy gap (ΔE) of 2.948 eV is associated to Ru-2 molecule while Ru-1 complex is observed to have ΔE of 2.897 eV which affirms high kinetic stability and less reactivity of Ru-2 compound. However, as clearly shown in Fig. 2 and Table 2 the delocalization of electrons from HOMO to LUMO is more prominent in Ru-2 system with higher electron-donating capacity of − 5.053 than Ru-1 compound with nucleophilicity of − 5.043 eV respectively [33]. These implies that the ease of realising electron from Ru-2 compound to the target receptor site is comparably higher than Ru-1 molecule. The chemical hardness and softness of the studied Ruthenium polypridyl complexes were calculated using the formula below;

$$\text{Chemical hardness}(\eta) = \frac{1}{2}\left(E_{LUMO} - E_{HOMO}\right) \equiv \frac{1}{2}(\mathrm{I.P} - \mathrm{A}) \tag{5}$$

$$\text{Chemical softness}(S) = \frac{1}{2\eta} \equiv \frac{1}{(I.P - A)} \equiv \frac{1}{(E_{LUMO-E_{HOMO}})} \tag{6}$$

Chemical hardness suggests the resistivity of a molecule towards electron transfer, this implies that a high chemical hardness value is inversely proportional to low resistance of a molecule towards electron transfer. As such the η of 1.474 corresponds high *S* of 0.678 for Ru-2 compound, affirming the ease of electron transfer from Ru-2 molecule to the receptor target site which is in agreement to the docking studies of the said molecule [34].

3.4 Stabilization Energy Analysis

Natural bond orbital analysis (NBO) seeks to elucidate the mechanism of charge transfer between intra and intermolecular orbital bonding, conjugative and hyper-conjugative interaction, as well as the stabilization energies of the complexes [36]. NBO analysis of the studied molecules performed using NBO version 3.1 embedded in Gaussian 09 W package at DFT/B3lyp/Gen level of theory [37]. The strength of interaction between the donor- acceptor moiety is characterized by the stabilization energy $E^{(2)}$ of the studied complexes. So to say, the more intense the donor–acceptor orbital interaction explicated by the second order perturbation energy $E^{(2)}$, the more stable the complex might likely be. Correspondingly, the donor–acceptor $E^{(2)}$ (i−j) for nucleophilic (i) and electrophilic (j) moieties are calculated using the equation;

$$\mathrm{E}(2) = \mathrm{qi}\frac{(Fi,j)2}{Ej - Ei}$$

where qi designate the orbital occupancy, i,j represent the fock diagonal elements and Fi,j denote the off-diagonal fock matrix for the studied systems. As such, the large value of stabilization energy in kcal/mol obtained for the studied molecules is directly proportional to the increase in conjugation magnitude. From the result in Table 3, the interaction for both systems is predominated by mostly $\pi^* \rightarrow \pi^*$ interaction with a total stabilization energy of 1265.32 kj/

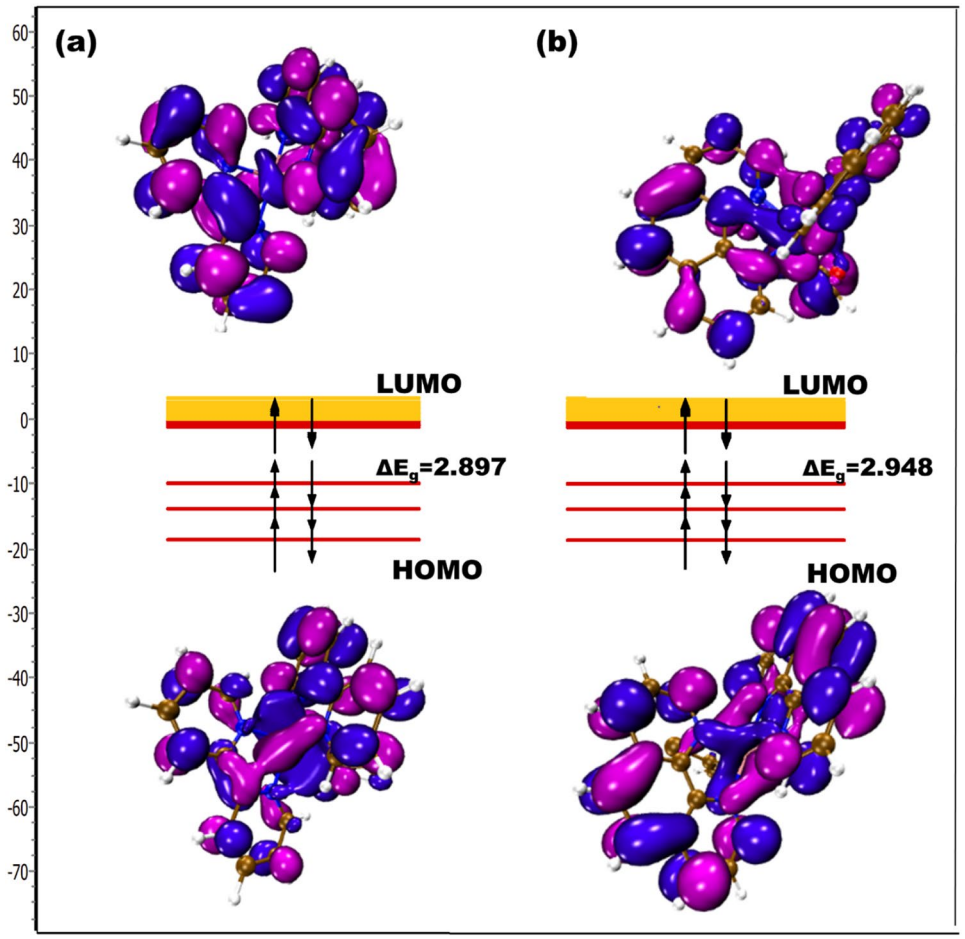


Fig. 2 Frontier molecular orbital isosurface values (0.02) of the studied compounds **a** Ru-1 and **b** Ru-2

Table 2 Electronic key parameters of frontier molecular orbital (FMO) energies and chemical quantum reactivity parameters of the studied ruthenium polypyridyl complex [35] calculated at B3LYP-D3BJ/gen/def2tzvp/LanL2DZ level of theory

Compounds	HOMO	LUMO	ΔE_g	IP	A	χ	μ	η	S	ω
Ru-1	− 5.043	− 2.146	2.897	5.043	2.146	1.449	− 3.595	1.449	0.690	9.363
Ru-2	− 5.053	− 2.105	2.948	5.053	2.105	1.474	− 3.579	1.474	0.678	4.345

mol for Ru-1 molecule and 1437. 33 kcal/mol for Ru-2 molecule. π*C19-C24 donor interaction gave the maximum contributive donation to the outstanding stability of Ru-2 compound. High stability of lone pairs was observed in LP(1)N39 → LP*(4)Ru37, LP(1)N40 → LP*(4)Ru37 and LP(1)N37 → LP*(6)Ru33 for Ru-1 and Ru-2 respectively with stabilization energies of 147.56, 146.39 and 3.84 kj/mol for both systems [38]. The highest stabilization energies for both compounds were observed between $\pi^* \rightarrow \pi^*$ (π*C19-C24 → π*C20-C21) interaction for Ru-1 compound while the minimum second perturbation energy was observed between LP(1)N37 → LP*(6) Ru33 interaction for Ru-2 complex. Thus it can be deduced that from the above NBO result, the spatial orientation of the studied Ruthenium derivative arises from their individual stabilization energies $E^{(2)}$, with Ru-2 pyrimidine ring contributing mostly to the stability of the compound which is in agreement to other electronic and reactivity studies [39].

3.5 UV–Vis Spectroscopy

Electronic excitation from the highest occupied molecular orbital (HOMO) to the lowest unoccupied molecular orbital (LUMO) H → L and is primarily responsible for the excited state recorded for Ru-1 and Ru-2 molecules. As such, understanding these compounds excited state dynamics is crucial for the effective utilization as well as characterization of the investigated molecules at molecular level. Table 4 and figure S1 clearly depicts the findings of the various excitation analysis as carefully determined from the experimental

Table 3 Stabilization energies of Ru-1 and Ru-2 calculated at the B3LYP-D3BJ/gen/def2tzvp/LanL2DZ level of theory

S/No.	Donor NBO	Acceptor NBO	$E^{(2)}$/(kj/mol.)	E(j)-E(i)/a.u	F(i,j)/a.u
Ru-1					
1	LP(1)N39	LP*(4)Ru37	147.57	0.56	0.178
2	LP(1)N40	LP*(4)Ru37	146.39	0.56	0.177
3	π*C1-N39	π*C2-C3	152.13	0.05	0.75
4	π*C1-N39	π*C4-C5	193.59	0.05	0.086
5	π*C7-N38	π*C9-C10	181.46	0.06	0.086
6	π*C19-C24	π*C20-C21	397.77	0.02	0.074
7	π*C19-C24	π*C25-C26	340.37	0.02	0.073
Ru-2					
8	LP(1)N37	LP*(6)Ru33	3.85	0.43	0.028
9	π*C1-N35	π*C2-C3	41.44	0.04	0.073
10	π*C1-N35	π*C4-C5	173.38	0.05	0.089
11	π*C4-C5	π*C51-C52	304.46	0.01	0.069
12	π*C6-N34	π*C7-C8	152.88	0.05	0.071
13	π*C6-N34	π*C9-C10	246.52	0.05	0.090
14	π*C18-C19	π*C49-C50	308.77	0.01	0.069

Table 4 Electronic absorption data for the complexes recorded in methanol calculated at (TD)-DFT level of theory

Systems	Excitation	Experimental λmax	Extinction coefficient	Theoretical λmax	Energy	Oscillator strength	% Contribution	Assignment
Ru-1	Solvent **S0 → S1**	497	0.60	− 5641.66	− 0.2198	− 0.0620	**H → L 204%**	n → π *
		446	0.69					
		342	1.36					
		293	4.05					
		247	3.16					
Ru-2	Solvent **S0 → S1**	489	1.15	− 5631.55	− 0.2196	− 0.0610	**H → L 204%**	n → π *
		445	1.15					
		267	4.03					
		226	4.03					
		204	3.94					

as well as TD-DFT calculations respectively [40]. In detail, comparison of the various atomic contributions from each chemical orbital to the HOMO and LUMO electron densities as well as λ_{max} and their various theoretical counterpart are highlighted herein. With respect to the obtained experimental maximum for both substances which were observed to occur at the visible range between 400 and 700 nm, suggest a close agreement of the experimental result with theoretically obtained λ_{max}, which was seen to occur between 5641.66 and 5631.55 nm respectively. Thus, according to the result obtained from the UV–visible spectroscopic studies, excitation of both studied ruthenium compounds from solvent phase was observed to be primarily, predominated by lone pairs (n), pi antibonding (π^*) orbitals. This observation, is due to the availability of lone pairs on both HOMO regions of the participating atoms, which explains the presence of extraordinary electron density at the nitrogen and ruthenium atoms [41]. Nonetheless, with over 204% percentage contribution H → L transition is primarily responsible for delocalization observed for both systems. Furthermore, electron delocalization from Lumo to Homo was observed, with a corresponding percentage contribution of about 6.603% respectively. Interestingly, result further reveal that the electronic spectra of the studied ruthenium complexes contain a typical metal to ligand charge transfer (MLCT) transition at the visible range of 497 nm for Ru-1 and 489 nm for Ru-2 respectively [42]. Due to the destabilization of the Ru-Homo–Lumo ("t2g-type" orbital), which in turn reduces the HOMO–LUMO gap and the energy of the MLCT transition, the complexes 1 MLCT bands were red shifted in comparison to the prototype Ru-2 complex $[Ru(bpy)_3]^{2+}$ (^{1}MLCT at 450 nm). Thus, this observation is conspicuously shown in

Figure S1. At 293 and 267 nm respectively, were an intense ligand-centred transition in the UV region were observed to occur. In addition, CHP centring was observed to correspond to a sharp band ranging between 340 and 360 nm respectively, which elucidates that, the presence of low energy excitation correlates with the less negative reduction potential of the coordinated CHP, with respect to bipyridal (bpy) or phenyl (phen) moiety, which implies that π^* molecular orbitals (MOs) of CHP also possesses lower energy.

3.6 Vibrational Analysis

Fourier transform infrared is the most resourceful tool for molecular characterization with diverse application in pharmaceutical, plastics and polymer industry due to its sensitivity, fastness and simplicity. The vibrational properties of Chp, Ru-1, Ru-2 molecules were calculated theoretically to compare with already obtained experimental counterparts [43]. The studied compounds were observed to exhibit 4 and 8 modes of vibrations for all studied systems [44]. FT-IR studies reveal that Ru-1 and Ru-2 molecules have similar number of 273 electrons and 52 atoms respectively. As such, the calculated result explicated that the computed frequencies which is attributed to their harmonic nature and different orientation in space [45]. Nevertheless, the observed frequencies all correspond within the estimated range.

3.6.1 C–C, CH Vibration

The weak absorption peaks at 1620–1680 cm^{-1}, 2800–2700 cm^{-1} are mostly assigned to C–C and CH group. CH stretching vibration of CH group is found to occur at 1624, 1589, 3122 and 2839 cm^{-1} absorption peaks from the experimental IR spectrum, whereas the calculated frequencies were observed to occur at 1616, 1631, 2999 and 3172 cm^{-1} wavenumbers respectively. However, at 1624, 1589 and 1441 cm^{-1} absorption peaks, bending deformation of scissoring was observed in the experimental IR spectra corresponding to the calculated vibration at 1616, 1631 and 1452 for CH group. Result explicated that at 1616, 1631 and 3172 cm^{-1} absorption intensities C=O stretching vibrational mode was observed for chp, Ru-1 and Ru-2 compounds respectively [46]. The peaks at 1616, 1631 and 3172 cm^{-1} wavenumbers are assigned to C=C bonds absorption of the alkene group for all studied molecules respectively. As such the deformation bands corresponding to C=C aromatic alkene group from the experimental IR spectrum is observed to occur at 1600, 1377, 835, 719 and 557 cm^{-1} absorption peaks. C=C twisting, rocking and wagging bending deformation was observed to occur at a high absorption intensity of 1371, 1370, 1587 and 556 cm^{-1} from the calculated IR spectra analysis for Chp, Ru-1 and Ru-2 complexes respectively [47].

3.6.2 C = O Vibration

The weak absorption peak at 1740–1720 cm^{-1} frequencies wer assigned to CO stretching vibration of the carbonyl group. The absorption of C=O group was observed to occur at 1377 cm^{-1} from the experimental IR spectra which correspond to a high absorption intensity of 1378 cm^{-1} wavenumber, while the result from the calculated IR spectra for the carbonyl group was observed to occur at a weak absorption intensity of 1393, 1390 cm^{-1} frequencies for Ru-1 and Ru-2 molecules respectively [48]. Thus, the results explicated that the calculated frequencies are slightly greater than the experimental frequencies which could be attributed to the harmonic nature and possibly the slight difference in the orientation of the studied molecules in space. This results is presented on Table 5.

3.7 Molecular Docking

The application of Ru-1 and Ru-2 molecules as an effective anti-tuberculosis drug were evaluated using molecular

Table 5 Summary of FT-IR Spectra of the complexes (wavenumber in cm^{-1}) calculated at B3LYP-D3BJ/gen/def2tzvp/LanL2DZ level of theory

Compounds	Modes	XRD Infrared frequency	Theoretical calculated freq	Assignment
Chp	1	3325	3290	Vassy CH
	2	3122	2999	VssyCH
	3	1624	1616	VssyC=C, σCH
	4	1600	1587	ϒCH
Ru-1	1	2974	3182	Vassy CH
	2	2839	3174	VssyCH
	3	1589	1631	VssyC=C, σCH
	4	1441	1452	σCH
	5	1377	1390	VssyC=O
		1377	1370	ϒCH
	6	835	854	βCH
	7	719	714	αC=C
	8	557	556	αC=C, ϒCH
Ru-2	1	2974	3183	Vassy CH
	2	2839	3172	VssyCH
	3	1589	1631	VssyC=C, σCH
	4	1441	1453	σCH
	5	1377	1393	VssyC=O
	6	1377	1371	ϒCH
	7	835	852	βCH
	8	719	**714**	αC=C
	9	557	**556**	αC=C, ϒCH

σ scissorying, ϒ = Rocking bending deformation, β = twisting bending deformation, α = wagging bending deformation

docking experiment alongside several tuberculosis proteins. The result obtained from the docking studies were compared with isoniazid standard drug as these drugs has been reported to be generally harmless and most effective drug used in the treatment of tuberculosis [49]. As such the lethal effect of isoniazid (INH) on mycobacterium tuberculosis (M.tb) is observed to be as a result of its interaction with the Kat G enzyme found in the cells of the mentioned pathogens. The following receptors 2nv6 and 5syj were docked with Ru-1 and Ru-2 ligands, as such the results of the best mode with interacting amino acid residues, binding affinities and interaction distances are carefully reported in Table 6 and Fig. 3 The result reveals a brilliant interaction between the studied Ru-1, Ru-2 ligands and the selected tuberculosis proteins. The binding score obtained after docking the proposed ligands with the selected 2nv6 and 5syj are − 8.6 and − 6.7 kcal/mol for Ru-1 complex. Similarly, the binding affinity of − 10.2 and − 7.5 kcal/mol was obtained when 2nv6 and 5syj proteins were docked with Ru-2 compound. However, when isoniazid was docked with both proteins, the binding score of − 6.0 was observed for 2nv6 receptor while no interaction was seen for 5syj following the low binding score of 0.0 kcal/mol. The obtained result evidently affirm that Ru-2 compound possess higher relatively binding affinity than Ru-1 and the standard drug, as such is expected to possess a comparably outstanding efficacy to inhibit the tuberculosis receptor and thus function as anti-tuberculosis agent. As shown in Table 6 It was observed that only one hydrogen bonding interaction was found for Ru-1 with 5syj while two hydrogen bonding interactions were observed for Ru-2 molecule at the interacting amino acid residues. Also, similar but slightly different scenario was observed for 2nv6 receptor, as two hydrogen bonding interactions were observed for Ru-1 whereas only one hydrogen bond interaction was seen for Ru-2 complex. Results further divulged that three interacting hydrogen bonds were observed when isoniazid was docked with 2nv6 protein at the interacting amino acid residues respectively. The strength of interaction as well as the efficacy of a proposed drug to a disease receptor is graded by the number of hydrogen bonds, binding affinity as well as other stabilizing interaction such as hydrophobic contacts, π-sulfur interaction, π -alkyl interaction and Van der Waals interactions [50]. Thus, our conclusion is that Ru-2 molecule exhibits a comparably outstanding binding result as elucidated from the docking experiment.

4 Conclusions

To effectively test the efficaciousness of ruthenium polypyridyl complexes Ru-1 and Ru-2 as anti-tubercular agent, a quantum chemical investigation approach was employed. The results obtained from the reactivity study demystify that Ru-2 molecule with energy gap of 2.948 eV and nucleophilicity of − 5.053 eV is unequivocally and comparably more stable than Ru-1 molecule with energy gap (E_g) of 2.897 eV and stabilization energy $E^{(2)}$ of 343.53 kcal/mol which was observed to be associated with nucleophilicity of − 5.043 eV respectively. Furthermore, the molecular docking studies reveals that Ru-2 compound binds more effectively with 2nv6 receptor than Ru-1 system with outstanding values of binding energy of − 10.2 and − 8.6 kcal/mol respectively. As a comparison, the predicted value of binding score for isoniazid (a commercial anti-tubercular agent), was − 6.0 kcal/mol with 2nv6 receptor. Ru-2 compound was also observed to bind more with 5syj receptor than the isoniazid

Table 6 Binding affinity and interacting amino acids for the different receptor proteins studied

5syj Receptor	Binding affinity	Interacting amino acids residues	Binding distance	2nv6 Receptor	Binding affinity	Binding distance	Interacting amino acids residues
Ru-1	− 6.7	B:GLY100:HN-:UNK0:O	2.95311	**Ru-1**	− 8.6	3.01713	A:ALA198:HN-:UNK0:O
		:UNK0:Cl-:UNK0(hydrophobic)	3.98495			3.54955	A:ILE16:CG2-:UNK0
Ru-2	− 7.5	:UNK0:C-B:PHE375:O	3.57779	**Ru-2**	− 10.2	2.17172	A:GLY96:HN-:UNK0:O
		:UNK0:C-B:PHE375:O	3.55772			3.72777	A:ILE16:CG2-:UNK0 (Hydrophobic)
Isoniazid	− 0.0	–	–	Isoniazid	− 6.0	2.037	:UNK1:H-A:GLY96:O
		–	–			2.98944	:UNK1:H-A:GLY96:O
		–	–			3.72461	:UNK1:C-A:LEU63:O

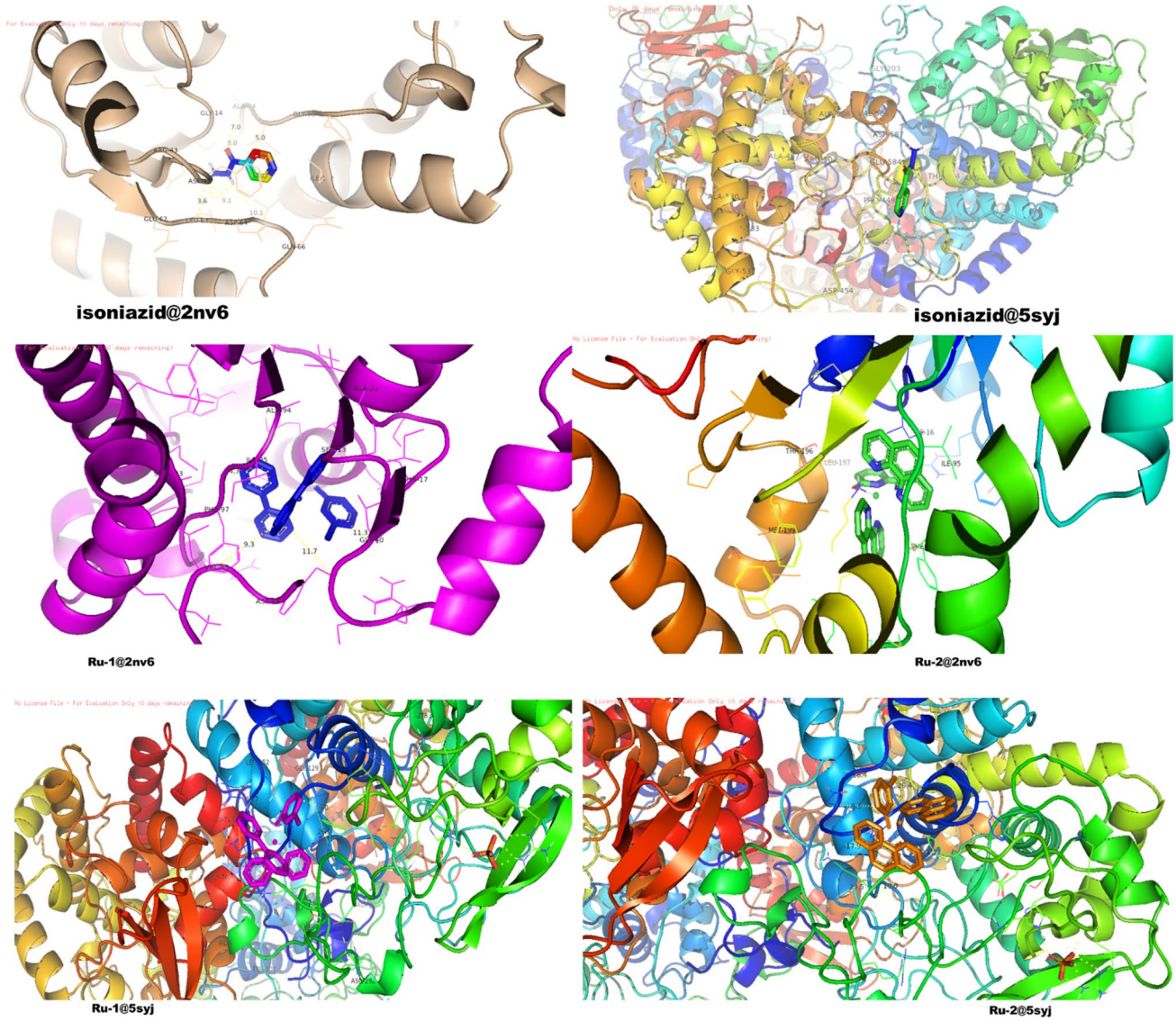


Fig. 3: 3D representations of the docked conformers of the studied compounds

as well as Ru-1 complex with a comparably high binding score of − 7.5 kcal/mol which suggests that Ru-2 molecule possess the potency to completely inhibit the growth of neutrophil granulocytes by releasing electrons as elucidated by nucleophilicity of − 5.053 eV in attempt to curb the further growth of aforementioned tuberculosis receptors. Thus, the proposed Ru-2 molecule could be a more suitable and effective anti-tuberculosis agent and hence can be applied in related cases.

Supplementary Information The online version contains supplementary material available at https://doi.org/10.1007/s42250-023-00769-2.

Acknowledgements We are grateful to the Institute of International Education of the United States for the Fulbright Fellowship. The authors would like to acknowledge the center for high performance computing (CHPC), South Africa for providing computational resources for this research project.

Author Contributions AOR: investigation, methodology, funding acquisition, validation, formal analysis, writing—original draft. JAO: conceptualization, visualization, resources, supervision. HL: investigation, formal analysis, writing—review and editing. SOA: investigation, formal analysis, writing—review and editing. AAA: investigation, formal analysis, writing. WAO: supervision, project administration, Writing—review and editing. GEM and MER: analysis and writing. AL: writing—review and editing. A-LM: computational resources.

Data availability All data are contained within the manuscript and electronic supporting information (ESI).

Declarations

Conflict of interest The authors declare that they have no known competing financial interests or personal relationships that could have appeared to influence the work reported in this paper.

References

1. Kumar V, Abbas AK, Fausto N, Mitchell RN (2007) Robbins Basic Pathology, 8th edn. Saunders Elsevier, pp 516–522
2. Ducati RG, Ruffino-Netto A, Basso LA, Santos DS (2006) The resumption of consumption: a review on tuberculosis. Mem Inst Oswaldo Cruz 101(7):697–714
3. DeVille K (1989) Robert koch: a life in medicine and bacteriology. Bioscience 39(7):493–495
4. Sahin C (2022) Synthesis, characterization, photophysical and electrochemical properties of pyridine based ruthenium complexes. Düzce Univ J Sci Technol 10(1):207–215. https://doi.org/10.29130/dubited.956216
5. Qian BF, Wang JL, Jia AQ, Shi HT, Zhang QF (2021) Syntheses, reactivity, structures and photocatalytic properties of mononuclear ruthenium(II) complexes supported by 1,4,7-trimethyl-1,4,7-triazacyclononane (Me3tacn) ligands". Inorganica Chim Acta 516:120128
6. Zeng L, Gupta P, Chen Y, Wang E, Ji L, Chao H, Chen ZS (2017) The development of anticancer ruthenium (II) complexes: from single molecule compounds to nanomaterials. Chem Soc Rev 46(19):5771–5804
7. Lapasam A, Banothu V, Addepally U, Kollipara MR (2019) Half-sandwich arene ruthenium, rhodium and iridium thiosemicarbazone complexes: synthesis, characterization and biological evaluation. J Chem Sci 132:1
8. Dömötör O, Enyedy ÉA (2019) Binding mechanisms of half-sandwich Rh (III) and Ru (II) arene complexes on human serum albumin: a comparative study. J Biol Inorg Chem 24:703–719
9. Lenis-Rojas OA, Fernandes AR, Roma-Rodrigues C, Baptista PV, Marques F, Pérez-Fernández D, Guerra-Varela J, Sánchez L, Vázquez-García D, Torres ML, Fernández A (2016) Heteroleptic mononuclear compounds of ruthenium (II): synthesis, structural analyses, in vitro antitumor activity and in vivo toxicity on zebrafish embryos. Dalton Trans 45(47):19127–19140
10. Yu Q, Liu Y, Xu L, Zheng C, Le F, Qin X, Liu Y, Liu J (2014) Ruthenium (II) polypyridyl complexes: cellular uptake, cell image and apoptosis of HeLa cancer cells induced by double targets. Eur J Med Chem 23(82):82–95
11. Sahin C, Dittrich T, Varlikli C, Icli S, Lux-Steiner MC (2010) Role of side groups in pyridine and bipyridine ruthenium dye complexes for modulated surface photovoltage in nanoporous TiO2. Solar Energy Mater Solar Cells 94(4):686–90
12. Louis H, Mathias GE, Unimuke TO, Emori W, Ling L, Owen AE, Adeyinka AS, Ntui TN, Cheng CR (2022) Isolation, characterization, molecular electronic structure investigation, and in-silico modeling of the anti-inflammatory potency of trihydroxystilbene. J Mol Struct 15(1266):133418
13. Liang W, Luo X (2020) Theoretical studies of MoS2 and phosphorene drug delivery for antituberculosis drugs. J Phys Chem C 124(15):8279–87
14. Zhang Z, Wang Q, Xue J, Du Y, Liu J, Hong Z (2020) Vibrational spectroscopic investigation into novel ternary eutectic formed between pyrazinamide, fumaric acid, and isoniazid. ACS Omega 5(28):17266–74
15. Garg A, Borah D, Trivedi P, Gogoi D, Chaliha AK, Ali AA, Chetia D, Chaturvedi V, Sarma D (2020) A simple work-up-free, solvent-free approach to novel amino acid linked 1, 4-disubstituted 1, 2, 3-triazoles as potent antituberculosis agents. ACS Omega 5(46):29830–7
16. Frisch MJ, Trucks GW, Schlegel HB, Scuseria GE, Robb MA, Cheeseman JR, Scalmani G, Barone V, Mennucci B, Petersson GA, Nakatsuji H (2009) Gaussian 16. Gaussian Inc, Wallingford
17. Dennington R, Keith TA, Millam JM (2016) GaussView 6.0. 16. Semichem Inc, Shawnee Mission
18. Farrugia LJ (1997) ORTEP-3 for Windows-a version of ORTEP-III with a Graphical User Interface (GUI). J Appl Crystallogr 30(5):565
19. Hanwell MD, Curtis DE, Lonie DC, Vandermeersch T, Zurek E, Hutchison GR (2012) Avogadro: an advanced semantic chemical editor, visualization, and analysis platform. J Cheminf 4(1):1–7
20. Asogwa FC, Agwamba EC, Louis H, Muozie MC, Benjamin I, Gber TE, Mathias GE, Adeyinka AS, Ikeuba AI (2022) Structural benchmarking, density functional theory simulation, spectroscopic investigation and molecular docking of N-(1H-pyrrol-2-yl) methylene)-4-methylaniline as castration-resistant prostate cancer chemotherapeutic agent. Chem Phys Impact 5:100091
21. Trott O, Olson AJ (2010) AutoDock Vina: improving the speed and accuracy of docking with a new scoring function, efficient optimization, and multithreading. J Comput Chem 31(2):455–61
22. Dassault Systemes (2020) Discovery Studio Visualizer. Dassault Systeme Biovia Corp, 2020
23. The PyMOL Molecular Graphics System, Version 1.2r3pre, Schrodinger LLC (2015) Available: https://pymol.org
24. Osigbemhe IG, Oyoita EE, Louis H, Khan EM, Etim EE, Edet HO, Ikenyirimba OJ, Oviawe AP, Obuye F (2022) Antibacterial potential of N-(2-furylmethylidene)-1, 3, 4-thiadiazole-2-amine: Experimental and theoretical investigations. J Indian Chem Soc 99(9):100597
25. Eno EA, Patrick-Inezi FA, Louis H, Gber TE, Unimuke TO, Agwamba EC, Ikenyirimba OJ, Akpanke JA, Oyoita E, Ejiofor EU, Adalikwu SA (2022) Theoretical investigation and antineoplastic potential of Zn (ii) Complexes of 6-Methylpyridine-2-carbaldehyde-N (4)- ethylthiosemicarbazone. Chem Phys Impact 5:100094
26. Jaziri E, Louis H, Gharbi C, Unimuke TO, Agwamba EC, Mathias GE, Fugita W, Nasr CB, Khedhiri L (2022) Synthesis, X-ray crystallography, molecular electronic property investigation, and leukopoiesis activity of novel 4, 6-dimethyl-1, 6-dihydropyridin-2-amino nitrate hybrid material. J Mol Struct 1268:133733
27. Louis H, Mathias GE, Ikenyirimba OJ, Unimuke TO, Etiese D, Adeyinka AS (2022) Metal-doped Al12N12X (X = Na, Mg, K) nanoclusters as nanosensors for carboplastin: insight from first-principles computation. J Phys Chem 126(27):5066–5080
28. Mohammadi MD, Abbas F, Louis H, Mathias GE, Unimuke TO (2022) Trapping of CO, CO2, H2S, NH3, NO, NO2, and SO2 by polyoxometalate compound. Comput Theor Chem 1215:113826
29. Mohammad MD, Abdullah HY, Louis H, Mathias GE (2022) 2D boron nitride material as a sensor for H2SiCl2. Comput Theor Chem 1213:113742
30. Osigbemhe IG, Oyoita EE, Louis H, Khan EM, Etim EE, Edet HO, Ikenyirimba OJ, Oviawe AP, Obuye F (2022) Antibacteria potential of N-(2-furylmethylidene)-, 3, 4-thiadiazole-2-amine: experimental and theoretical investigations. J Indian Chem Soc 99(9):100597
31. Louis H, Ifediora LP, Enudi OC, Unimuke TO, Asogwa FC, Moshood YL (2021) Evaluation of the excited state dynamics, photophysical properties, and the influence of donor substitution in a donor-pi-acceptor system. J Mol Model 27(10):1–18
32. Tuberculosis (2020) WHO Global Tuberculosis Report 2019. https://www.who.int/teams/global-tuberculosis-programme/tb-reports/global-tuberculosis-report-2020. Accessed 18 Aug 2022
33. Rawat P, Singh RN, Ranjan A, Ahmad S, Saxena R (2017) Antimycobacterial, antimicrobial activity, experiment (FT-IR,

FT-Raman, NMR, UV-Vis DSC) and DFT (transition state, chemical reactivity, NBO NLO) studies on pyrrole-isonicotinyl hydrazine. Spectrochim Acta Part A Mol Biomol Spectrosc 179:1–10
34. Anderson RF, Shinde SS, Maroz A, Boyd M, Palmer BD, Denny WA (2008) Intermediates in the reduction of the antituberculosis drug PA-824, (6S)-2-nitro-6-{[4-(trifluoromethoxy) benzyl] oxy}-6, 7-dihydro-5H-imidazole [2, 1-b] [1,3] oxazine, in aqueous solution. Org Biomol Chem 6(11):1973–1980
35. Liang J, Zhang X, Wang N, Chang T, Cui HL (2020) Vibrational spectra of pyrazinamide and isoniazid studied by terahertz spectroscopy and density functional theory. Spectrochim Acta Part A Mol Biomol Spectrosc 228:117591
36. Govindarajan M, Karabacak M, Suvitha A, Periandy S (2012) FT-IR, FT-Raman, ab initio, HF and DFT studies, NBO, HOMO-LUMO and electronic structure calculation on 4-chloro-3-nitrotoluene. Spectrochim Acta Part A Mol Biomol Spectrosc 89:137–148
37. Majerz I (2012) Directionality of inter-and intramolecular OHO hydrogen bonds: DFT study followed by AIM and NBO analysis. J Phys Chem A 116(30):7992–8000
38. Isravel AD, Jeyaraj JK, Thangasamy S, John WJ (2021) Comput Theor Chem 1202:113296
39. Emamian S (2016) How the mechanism of a [3 +2] cycloaddition involving a stabilized N-lithiated azomethineylide towards a π-deficient alkene is changed to stepwise by solvent polarity? What is the origin of its region-and endo stereospecificity? A DFT study using NBO, QTAIM and NCI Analyses. RSC Adv 6(79):75299–75314
40. Rad AS, Ardjmand M, Esfahani RM, Khodashenas B (2021) DFT Calculation towards the geometry optimization, electronic structure, infrared spectroscopy and UV-vis analyses of Favipiravir adsorption on the first-row transition metals doped fullerenes; a new strategy for COVID-19 therapy. Spectrochim Acta Part A Mol Biomol Spectrosc 247:119082
41. Da Silva HC, De Souza LA, Santos HF, De Almeida WB (2020) Determination of anticancer Zn(ii)-rutin complex structures insolution through density functional theory calculations of ^{1}H NMR and UV-VIS spectra. ACS Omega 5(6):3030–3042
42. Olajumoke A, Suleiman O, Odoh SO (2021) Copper-oxo active sites for methane C-H activation in Zeolite: molecular understanding of methane hydroxylation on UV-Vis spectra. Inorg Chem 60(12):8489–8499
43. Urbina F, Batra K, Luebke KJ, White JD, Matsiev D, Oison LL, Malerich JP, Hupcey MAZ, Madrid PB, Ekins S (2021) UV-adVISor: attention-based recurrent neutral networks to predict UV-Vis spectra. Anal Chem 93(48):16076–16085
44. Zhang Y, Zhang J, Wang H, Yang W, Wang C, Peng Y, Chen J, Li J, Gao F (2022) Selective catalytic reduction of NOx with NH3 over Cu/SSZ-13: elucidating dynamics of Cu active sites with in situ UV-Vis spectroscopy and DFT calculations. J Phys Chem C 126(20):8720–8733
45. Fang L, Shi Q, Nguyen J, Wu B, Wang Z, Lo I (2017) Removal mechanism of phosphate by lanthanum hydroxide nanorods: investigations using EXAFS, ATR-FTIR, DFT and surface complexation modeling approaches. Environ Sci Technol 51(21):12377–12384
46. Luo J, Hu C, Meng X, Crittenden J, Qu J, Peng P (2017) Antimony removal from aqueous solution using novel α-MnO2 nanofibers: equilibrium, kinetic, and density functional theory studies. ACS Sustain Chem Eng 5(3):2255–2264
47. Holdren S, Tsyshevsky R, Fears K, Owrutsky J, Wu T, Wang X, Eichhorn BW, Kuklja MM, Zachariah MR (2018) Adsorption and destruction of the G-series nerve agent simulant dimethyl methylphosphonate on zinc oxide. ACS Catal 9(2):902–911
48. Rhodes C, Lappi S, Fischer D, Sambasivan S, Genzer J, Franzen S (2008) Characterization of monolayer formation on aluminum-doped zinc oxide thin films. Langmuir 24(2):433–440
49. Reyes YI, Franco FC (2019) DFT study on the effect of proximal residues on the mycobacterium tuberculosis catalase-peroxidase (KatG) heme compound I intermediate and its bonding interaction with isoniazid. R Soc Chem. https://doi.org/10.1039/c9cp01465a
50. Agwupuye JA, Neji PA, Louis H, Odey JO, Unimuke TO, Bisiong EA, Eno EA, Utsu PM, Ntui TN (2021) Investigation on electronic structure, vibrational spectra, NBO analysis, and molecular docking studies of aflatoxins and selected emerging mycotoxins against wild-type androgen receptor. Heliyon 7(7):e07544

Springer Nature or its licensor (e.g. a society or other partner) holds exclusive rights to this article under a publishing agreement with the author(s) or other rightsholder(s); author self-archiving of the accepted manuscript version of this article is solely governed by the terms of such publishing agreement and applicable law.